



Cite this: *RSC Adv.*, 2018, 8, 26266

Immunomagnetic separation and size-based detection of *Escherichia coli* O157 at the meniscus of a membrane strip†

Hyeonjeong Lee, Jeongin Hwang, Yunsung Park,  Donghoon Kwon, Sanghee Lee, Inseok Kang and Sangmin Jeon *

We developed a facile method for the detection of pathogenic bacteria using gold-coated magnetic nanoparticle clusters (Au@MNCs) and porous nitrocellulose strips. Au@MNCs were synthesized and functionalized with half-fragments of *Escherichia coli* O157 antibodies. After the nanoparticles were used to capture *E. coli* O157 in milk and dispersed in a buffer solution, one end of a test strip was dipped into the solution. Due to the size difference between the *E. coli*-Au@MNC complexes (approximately 1 μm) and free Au@MNCs (approximately 180 nm), only *E. coli*-Au@MNC complexes accumulated at the meniscus of the test strip and induced a color change. The color intensity of the meniscus was proportional to the *E. coli* concentration, and the detection limit for *E. coli* in milk was 10^3 CFU mL⁻¹ by the naked eye. The presence of *E. coli*-Au@MNC complexes at the meniscus was confirmed using a real-time PCR assay. The developed method was highly selective for *E. coli* when compared with *Salmonella typhimurium*, *Listeria monocytogenes*, and *Staphylococcus aureus*.

Received 3rd June 2018

Accepted 18th July 2018

DOI: 10.1039/c8ra04739a

rsc.li/rsc-advances

Introduction

Foodborne illnesses that are frequently caused by pathogenic bacteria are a major public health concern worldwide. Since microorganisms can contaminate foods at any point during handling, prevention of foodborne illness requires rigorous inspection. Considering the short time before each meal, conventional cultivation techniques that require a lengthy period of time for bacterial cell culture are not suitable for field tests. Instrument-related methods that do not require bacterial cell culture have been developed and include quartz crystal microbalance,^{1,2} surface plasmon resonance,^{3,4} surface-enhanced Raman scattering,^{5,6} fluorescence spectroscopy,^{7,8} electrochemical sensors,⁹ and polymerase chain reaction.^{10–12} Although these techniques enable the detection of bacteria within a few hours, they require expensive instruments and experienced technicians.

In contrast, the lateral flow immunoassay (LFIA) uses a series of membrane pads, such as a sample pad, a conjugation pad containing antibody-functionalized gold nanoparticles, a nitrocellulose (NC) membrane with antibodies immobilized at test and control lines, and an absorbent pad. The presence of target bacteria is determined by observing a color change at the test and control lines caused by the accumulation of the Au nanoparticles.^{13–17} The LFIA is economical, disposable and easy to

use.^{16,18–22} However, the presence of high concentrations of food debris in food samples impedes sensitive measurement.

The sensitive and selective detection of foodborne bacteria may be achieved by adopting antibody-conjugated magnetic nanoparticles to separate target bacteria from food debris. After magnetic separation of target bacteria from a sample solution, the concentration of target bacteria can be determined either by a size sorting method,^{23,24} an electrochemical method,^{25,26} or by a sandwich assay using probes to which the specific detection antibody has been conjugated, such as fluorescence dyes and catalytic enzymes.^{27–30} Since the use of additional probes for a sandwich assay is a time-consuming and expensive process, a size sorting method is preferred for screening purposes.

Conventional size sorting methods utilize membrane filters to separate large bacteria-magnetic nanoparticle complexes from small free magnetic nanoparticles. The combination of membrane filters and magnetic nanoparticles offers an easy and cost-effective method of detection of foodborne bacteria.²⁴ However, it has a critical drawback. The sample solution dropped on a membrane filter flows down and spreads laterally, which increases the contact area with the solution and degrades the detection sensitivity. The contact area can be reduced by dispensing the solution using a fine nozzle or making the membrane surface hydrophobic. However, the use of fine nozzles increases the analysis time and the hydrophobic coating increases nonspecific binding.

We overcame these limitations by separating bacteria-magnetic nanoparticle complexes and free magnetic nanoparticles at the meniscus of a test strip. The test strip was prepared by simply overlapping an absorbent pad on an NC

Department of Chemical Engineering, Pohang University of Science and Technology (POSTECH), 77 Cheongam-Ro, Nam-Gu, Pohang, Gyeongbuk, Republic of Korea. E-mail: jeons@postech.ac.kr

† Electronic supplementary information (ESI) available. See DOI: 10.1039/c8ra04739a



membrane with appropriate pore size. Half-antibody fragment-conjugated, Au-coated magnetic nanoparticle clusters (Au@MNCs) were used to capture *Escherichia coli* O157 in milk, followed by magnetic separation and dispersal in phosphate buffer (PB). The immersion of one end of the test strip in the solution containing the free Au@MNCs and Au@MNC–bacteria complexes induced a color change at the meniscus due to the accumulation of the Au@MNC–bacteria complexes. The detection limit for *E. coli* in milk was 10^3 colony forming units (CFU) mL^{-1} with the naked eye, which was superior to the typical LFIA (10^5 CFU mL^{-1}).^{31–34}

Experimental

Materials and reagents

Sodium citrate tribasic dihydrate, iron(III) chloride hexahydrate ($\text{FeCl}_3 \cdot 6\text{H}_2\text{O}$), urea, gold(III) chloride trihydrate ($\text{HAuCl}_4 \cdot 3\text{H}_2\text{O}$), sodium borohydride (NaBH_4), polyacrylamide, (3-aminopropyl) triethoxysilane (APTES), hydroxylamine hydrochloride ($\text{NH}_2\text{OH} \cdot \text{HCl}$), tris(2-carboxyethyl)phosphine (TCEP), potassium phosphate monobasic (KH_2PO_4), potassium phosphate dibasic (K_2HPO_4), bovine serum albumin (BSA), and Tween 20 were purchased from Sigma-Aldrich (St. Louis, MO, USA). Anti-*E. coli* O157:H7 antibody was purchased from KPL (Gaithersburg, MD, USA). Absorbent pads, NC membranes, and Amicon ultra-0.5 centrifugal filters were purchased from Millipore (Billerica, MA, USA). Real-time polymerase chain reaction (PCR) experiments were carried out using PowerChek™ EHEC real-time PCR kit (KogeneBiotech, Seoul, Korea) and analyzed using a QuantStudio™ 3 Real-Time PCR system (Applied Biosystems, Franklin Lakes, NJ, USA).

Preparation of antibody-conjugated Au@MNCs

Gold-coated superparamagnetic Fe_3O_4 nanoparticle clusters were synthesized as described elsewhere.^{35–37} In brief, 4 mmol of $\text{FeCl}_3 \cdot 6\text{H}_2\text{O}$, 12 mmol of urea, 8 mmol of sodium citrate tribasic dehydrate, and 0.4 g polyacrylamide were dissolved in 80 mL deionized (DI) water. After the solution was heated in a Teflon-lined autoclave at 200 °C for 10 h, the precipitate (MNC) was magnetically collected and rinsed several times with DI water. To coat the gold nanoparticles onto an MNC, amine groups were produced on the surface of the MNC by incubating 8 mg of MNC overnight in 40 mL of 1% APTES in ethanol. After washing the MNCs with ethanol and DI water, they were added to a solution of 14 nm gold nanoparticles and shaken for 5 h. Half fragments of anti-*E. coli* antibody were obtained by adding 40 μg of the antibody to 400 μL of PB containing 0.125 mM of TCEP for 1 h. The direct conjugation of half-antibody fragments to Au@MNCs via Au–S bonds provided the desired orientation of the antibody to efficiently capture target bacteria.^{38,39}

Results and discussion

Antibody-conjugated Au@MNCs

Fig. 1(a) presents a representative scanning electron microscopy (SEM) image of Au@MNCs. The bright spots correspond to Au

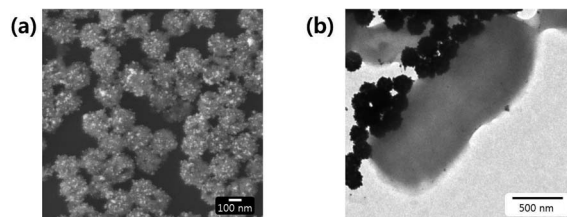


Fig. 1 (a) SEM image of Au@MNCs, wherein 14 nm gold nanoparticles appear as bright spots. (b) TEM image of *E. coli*–Au@MNC complexes.

nanoparticles. The mean diameter of Au@MNCs was 180 nm, and each MNC comprised hundreds of 14 nm magnetic nanoparticles. Fe_3O_4 nanoparticles larger than 30 nm exhibit ferromagnetism. Therefore, clusters of 14 nm Fe_3O_4 nanoparticles were used to maintain the paramagnetic property and allow the efficient magnetic separation of the nanoparticles. Fig. 1(b) displays a representative transmission electron microscopy image of *E. coli* covered with many Au@MNCs. The *E. coli*–Au@MNC complex was one order of magnitude larger than the Au@MNCs, which made it possible to separate the *E. coli*–Au@MNC complexes from the free Au@MNCs.

Detection of *E. coli*–Au@MNCs at the meniscus of the test strip

Fig. 2 illustrates the structure of the test strip, which comprises an absorbent pad and NC membrane. The NC membrane was pressed to generate a control line with considerably smaller pores compared to the initial membrane (see SEM images). As a result, the Au@MNC–bacteria complexes accumulated at the meniscus (*i.e.*, the test line) upon immersion of the test strip into a sample solution containing free Au@MNCs and *E. coli*–Au@MNC complexes, whereas the free Au@MNCs moved up and accumulated at the control line, with the smaller pores. The immersion of the test strip into a sample solution resulted in the formation of a meniscus line.

The line's shape changed depending on the width of the test strip. To examine the meniscus shape, a test strip with an NC membrane (HF180, Millipore) was dipped into a solution

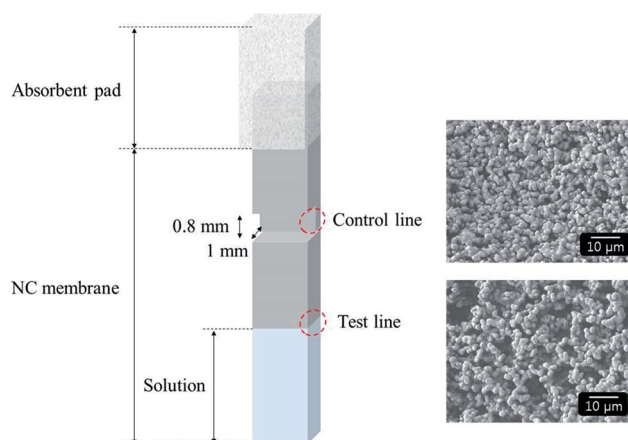


Fig. 2 Schematic of test strip with an NC membrane overlapped by an absorbent pad (left) and SEM images (right) showing the pores at the control line (upper) and test line (lower).



containing Au@MNCs. The meniscus became more curved and blurred as the width increased, which degraded the detection sensitivity (Fig. 3). Since handling the 2 mm-wide test strip was not convenient, the 3 mm-wide test strip was selected as the optimal membrane and was used throughout the experiments.

Interestingly, most *E. coli*-Au@MNC complexes accumulate at the meniscus and rarely accumulate below the meniscus. Numerical simulations were conducted using the COMSOL Multiphysics package to examine the accumulation of *E. coli*-Au@MNC complexes at the meniscus line. The permeability of the NC membrane was assumed to be 10^{-10} m^2 . The solution flowed toward the meniscus of the NC membrane and the flow velocity reached a maximum at the meniscus (Fig. 4). Thus, most *E. coli*-Au@MNC complexes in the solution would accumulate at the meniscus.

Detection of *E. coli* in milk

Antibody-conjugated Au@MNCs were incubated in 15 mL of *E. coli* O157-spiked milk at various concentrations (0 to 10^8 CFU mL^{-1}) and magnetically separated and dispersed in $200 \mu\text{L}$ of 0.1% Tween 20. The immersion of a test strip into the solution induced the absorption of free Au@MNCs and *E. coli*-Au@MNC complexes on the membrane. Fig. 5(a) shows optical images of the test strips after immersion for 3 min. The meniscus became darker with increasing *E. coli* concentration because of the

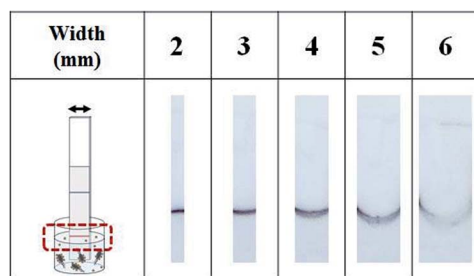


Fig. 3 Optical images of test strips after immersion in Au@MNC solution for 3 min. As the width of the test strip increases, the meniscus becomes more curved and blurred.

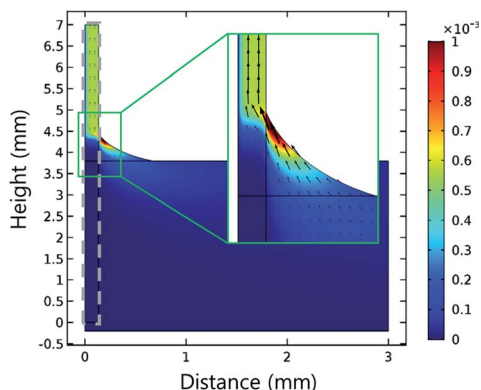


Fig. 4 Flow velocity distribution of water in contact with the NC membrane (dashed line) obtained using numerical simulations. Black arrows display the direction and magnitude of velocity field. The color bar indicates the magnitude of flow velocity (m s^{-1}).

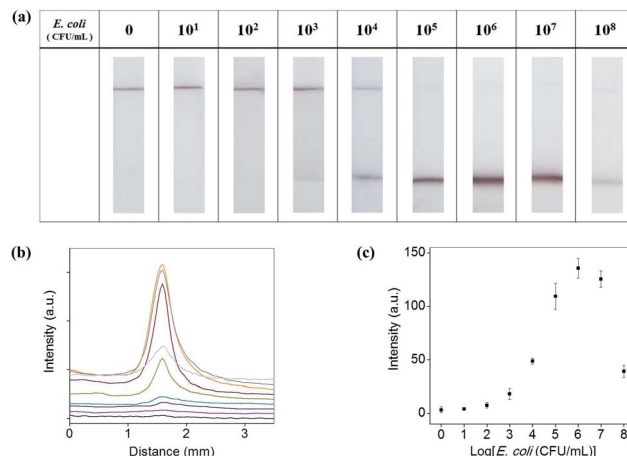


Fig. 5 (a) Optical images of test strips with the test line (lower line) and control line (upper line) after incubation for 3 min in *E. coli*-spiked milk at various concentrations ranging from 0 to 10^8 CFU mL^{-1} . (b) Variation in gray-scale intensities at the meniscus along the flow direction for *E. coli* concentration at 0 (black), 10 (violet), 10^2 (navy), 10^3 (cyan), 10^4 (olive), 10^5 (wine), 10^6 (orange), 10^7 (gray), and 10^8 (light gray) CFU mL^{-1} . (c) Maximum gray-scale intensities at the test line as a function of *E. coli* concentration (from three measurements).

increase in the number of *E. coli*-Au@MNC complexes in the solution. In contrast, the control line having a reduced pore size became paler with increasing *E. coli* concentration because of the decrease in the number of free Au@MNCs. Of note, the accumulation of *E. coli*-Au@MNC complexes occurred at the meniscus even though the test strip below the meniscus was fully immersed in the solution, which increased the assay sensitivity.

For quantitative analysis, the colors at the meniscus and control line were converted to a gray-scale value using ImageJ software (NIH, Bethesda, MD, USA). Fig. 5(b) shows the variation in the intensities at the meniscus along the flow direction and Fig. 5(c) shows the maximum intensities, both as a function of *E. coli* concentration. The intensity at the meniscus increased with increasing *E. coli* concentration and showed a maximum value at 10^6 CFU mL^{-1} . The decrease in intensity at concentrations above 10^6 CFU mL^{-1} may be attributed to the relative decrease (compared with *E. coli*) in the number of Au@MNCs ($\sim 10^8 \text{ mL}^{-1}$). At *E. coli* concentrations above 10^6 CFU mL^{-1} , a lower number of Au@MNCs bound to the surface of each *E. coli* bacterium, and the color at the meniscus became paler despite the accumulation of a greater number of complexes. The detection limit was determined to be 10^3 CFU mL^{-1} of *E. coli* in milk after 3 min of immersion, which is higher than the sensitivity of typical LFIA (10^5 CFU mL^{-1}).^{31–34} Table 1 shows that the sensitivity of our method is superior to other LFIAs for detection of *E. coli* O157.^{31–33,40–44}

E. coli detection using a real-time PCR assay

The presence of *E. coli* strains at the meniscus line was confirmed using a real-time PCR (RT-PCR) assay. Two test strips in Fig. 5(a) with 0 and 10^3 CFU mL^{-1} *E. coli* were used for the RT-PCR measurement. After carefully cutting 2 mm of the test strip containing the meniscus line or the control line, each sample



Table 1 Comparison of sensitivity for detection of *E. coli* O157:H7 using various LFIA

Method	Sample matrix	LOD (CFU mL ⁻¹)	References
Colorimetric LFIA	Milk	10 ⁶	31 and 32
	Ground beef	10 ⁵	33
Fluorometric LFIA	Defatted milk	10 ⁴	40
	2% DMSO	10 ⁵	41
TMB-enhanced LFIA	Ground beef	4 × 10 ²	42
	Milk	9 × 10 ²	43
Dual AuNP LFIA	Milk	10 ³	44
Size-sorting LFA	Milk	10 ³	This work

was immersed in 200 μL of DI water and sonicated for 10 min. Then, 5 μL of each solution was mixed with 15 μL of RT-PCR premix solution, and RT-PCR was conducted for 1.5 h. Amplification of VT2 genes in *E. coli* was observed only for samples containing the meniscus line with 10³ CFU mL⁻¹ *E. coli* (Fig. 6), indicating that the test strip successfully separated *E. coli*-Au@MNC complexes from free Au@MNCs.

Selectivity of the assay

To evaluate the assay selectivity, a control experiment was conducted. *E. coli* antibody-functionalized Au@MNCs were incubated in 15 mL of milk with 10⁵ CFU mL⁻¹ *Listeria monocytogenes*, *Salmonella typhimurium*, and *Staphylococcus aureus*. After the magnetic separation of the bacteria-Au@MNC

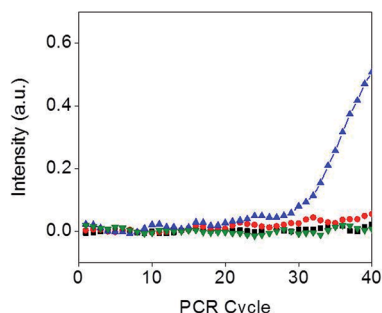


Fig. 6 Real-time amplification of VT2 genes obtained from the test strip containing the test line (black square) and the control line (red circle) after the experiment without *E. coli*, and the test strip containing the test line (blue triangle) and the control line (green inverted triangle) after the experiment with 10³ CFU mL⁻¹ *E. coli*.

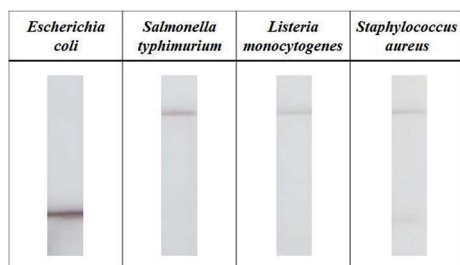


Fig. 7 Optical images of test strips for *Escherichia coli*, *Salmonella typhimurium*, *Listeria monocytogenes*, and *Staphylococcus aureus*. The bacterial concentration of each solution was 10⁵ CFU mL⁻¹ in milk.

complexes, they were dispersed in 200 μL of 0.1% Tween 20 and transferred into a 96-well plate. Fig. 7 shows optical images of the test strips after immersion in each solution for 3 min. A dark meniscus was observed for the test strip dipped into the *E. coli*-spiked sample, while a pale meniscus was observed for those treated with *S. typhimurium*, *L. monocytogenes*, and *Staph. aureus*, demonstrating the selectivity of this method.

Conclusions

In this study, we developed a novel method for the size-based detection of *E. coli* in milk. After immunomagnetic separation of *E. coli*, the immersion of the test strip in a solution containing free Au@MNCs and *E. coli*-Au@MNC complexes induced a color change at the meniscus due to the accumulation of the complexes. The accumulation at the meniscus occurred even though the test strip below the meniscus was fully immersed in the solution, which increased the assay sensitivity. The color intensity of the meniscus was proportional to the bacterial concentration (up to 10⁶ CFU mL⁻¹), and the detection limit was 10³ CFU mL⁻¹ for *E. coli* O157 in milk with the naked eye. The developed method has great potential to assess the presence of hazardous bacteria or heavy metal ions in drinking water simply by changing probe molecules.

Conflicts of interest

There are no conflicts to declare.

Acknowledgements

This work was supported by grants from the POSCO Research Fund (Project No. 2017Y018) and the National Research Foundation of Korea (NRF-2016R1A4A1010735).

Notes and references

- 1 Z. Farka, D. Kovář and P. Skládal, *Sensors*, 2015, **15**, 79.
- 2 Z. Shen, M. Huang, C. Xiao, Y. Zhang, X. Zeng and P. G. Wang, *Anal. Chem.*, 2007, **79**, 2312–2319.
- 3 Y. Wang, W. Knoll and J. Dostalek, *Anal. Chem.*, 2012, **84**, 8345–8350.
- 4 F. C. Dudak and İ. H. Boyacı, *Biotechnol. J.*, 2009, **4**, 1003–1011.
- 5 C. Fan, Z. Hu, A. Mustapha and M. Lin, *Appl. Microbiol. Biotechnol.*, 2011, **92**, 1053–1061.
- 6 H. Zhou, D. Yang, N. E. Mircescu, N. P. Ivleva, K. Schwarzmeier, A. Wieser, S. Schubert, R. Niessner and C. Haisch, *Microchim. Acta*, 2015, **182**, 2259–2266.
- 7 F. Mouffouk, A. M. Rosa da Costa, J. Martins, M. Zourob, K. M. Abu-Salah and S. A. Alrokayan, *Biosens. Bioelectron.*, 2011, **26**, 3517–3523.
- 8 L. Wang, W. Zhao, M. B. O'Donoghue and W. Tan, *Bioconjugate Chem.*, 2007, **18**, 297–301.
- 9 C.-X. Zhou, R.-J. Mo, Z.-M. Chen, J. Wang, G.-Z. Shen, Y.-P. Li, Q.-G. Quan, Y. Liu and C.-Y. Li, *ACS Sens.*, 2016, **1**, 965–969.



- 10 P. de Boer, H. Rahaoui, R. J. Leer, R. C. Montijn and J. M. B. M. van der Vossen, *Food Microbiol.*, 2015, **51**, 96–100.
- 11 Y. Zeng, Y. Wan and D. Zhang, *Microchim. Acta*, 2016, **183**, 741–748.
- 12 Y. Yang, F. Xu, H. Xu, Z. P. Aguilar, R. Niu, Y. Yuan, J. Sun, X. You, W. Lai, Y. Xiong, C. Wan and H. Wei, *Food Microbiol.*, 2013, **34**, 418–424.
- 13 J. E. Schonhorn, S. C. Fernandes, A. Rajaratnam, R. N. Deraney, J. P. Rolland and C. R. Mace, *Lab Chip*, 2014, **14**, 4653–4658.
- 14 A. K. Yetisen, M. S. Akram and C. R. Lowe, *Lab Chip*, 2013, **13**, 2210–2251.
- 15 D. H. Choi, S. K. Lee, Y. K. Oh, B. W. Bae, S. D. Lee, S. Kim, Y.-B. Shin and M.-G. Kim, *Biosens. Bioelectron.*, 2010, **25**, 1999–2002.
- 16 X. Mao, Y. Ma, A. Zhang, L. Zhang, L. Zeng and G. Liu, *Anal. Chem.*, 2009, **81**, 1660–1668.
- 17 S. Rong-Hwa, T. Shiao-Shek, C. Der-Jiang and H. Yao-Wen, *Food Chem.*, 2010, **118**, 462–466.
- 18 Y. Zhang, J. Bai and J. Y. Ying, *Lab Chip*, 2015, **15**, 1465–1471.
- 19 D. J. You, T. S. Park and J.-Y. Yoon, *Biosens. Bioelectron.*, 2013, **40**, 180–185.
- 20 G. A. Posthuma-Trumpie, J. Korf and A. van Amerongen, *Anal. Bioanal. Chem.*, 2009, **393**, 569–582.
- 21 J. Yan, Y. Liu, Y. Wang, X. Xu, Y. Lu, Y. Pan, F. Guo and D. Shi, *Sens. Actuators, B*, 2014, **197**, 129–136.
- 22 J. Hu, J. R. Choi, S. Wang, Y. Gong, S. Feng, B. Pingguan-Murphy, T. J. Lu and F. Xu, *Sens. Actuators, B*, 2017, **243**, 484–488.
- 23 H. Lee, T.-J. Yoon and R. Weissleder, *Angew. Chem., Int. Ed. Engl.*, 2009, **48**, 5657–5660.
- 24 W.-B. Shim, C.-W. Lee, M.-G. Kim and D.-H. Chung, *Anal. Methods*, 2014, **6**, 9129–9135.
- 25 C. Lulu, Z. Qi, D. Huang, F. Yingchun and L. Yanbin, *Electroanalysis*, 2018, **30**, 517–524.
- 26 Q. Zhang, L. Li, Z. Qiao, C. Lei, Y. Fu, Q. Xie, S. Yao, Y. Li and Y. Ying, *Anal. Chem.*, 2017, **89**, 12145–12151.
- 27 Y. Che, Y. Xu, R. Wang and L. Chen, *Anal. Bioanal. Chem.*, 2017, **409**, 4709–4718.
- 28 X.-L. Su and Y. Li, *Anal. Chem.*, 2004, **76**, 4806–4810.
- 29 Y. Zhao, M. Ye, Q. Chao, N. Jia, Y. Ge and H. Shen, *J. Agric. Food Chem.*, 2009, **57**, 517–524.
- 30 J. Joo, D. Kwon, H. H. Shin, K.-H. Park, H. J. Cha and S. Jeon, *Sens. Actuators, B*, 2013, **188**, 1250–1254.
- 31 C. Song, C. Liu, S. Wu, H. Li, H. Guo, B. Yang, S. Qiu, J. Li, L. Liu, H. Zeng, X. Zhai and Q. Liu, *Food Control*, 2016, **59**, 345–351.
- 32 M. S. Suria, A. T. Mohd Afendy, M. Noor Azlina and I. Zamri, *Int. Food Res. J.*, 2015, **22**, 2587–2593.
- 33 J. Wang, R. Katani, L. Li, N. Hegde, E. L. Roberts, V. Kapur and C. DebRoy, *Toxins*, 2016, **8**, 92.
- 34 P. Noguera, G. A. Posthuma-Trumpie, M. van Tuil, F. J. van der Wal, A. de Boer, A. P. H. A. Moers and A. van Amerongen, *Anal. Bioanal. Chem.*, 2011, **399**, 831–838.
- 35 W. Cheng, K. Tang, Y. Qi, J. Sheng and Z. Liu, *J. Mater. Chem.*, 2010, **20**, 1799–1805.
- 36 L. Wang, J. Bai, Y. Li and Y. Huang, *Angew. Chem., Int. Ed.*, 2008, **47**, 2439–2442.
- 37 J. Hwang, D. Kwon, S. Lee and S. Jeon, *RSC Adv.*, 2016, **6**, 48445–48448.
- 38 H. Sharma and R. Mutharasan, *Anal. Chem.*, 2013, **85**, 2472–2477.
- 39 D. Kwon, H. Yoo, H. Lee and S. Jeon, *Sens. Actuators, B*, 2018, **255**, 552–556.
- 40 Y. Zhao, H. Wang, P. Zhang, C. Sun, X. Wang, X. Wang, R. Yang, C. Wang and L. Zhou, *Sci. Rep.*, 2016, **6**, 21342.
- 41 C. Song, J. Liu, J. Li and Q. Liu, *Biosens. Bioelectron.*, 2016, **85**, 734–739.
- 42 I.-H. Cho, A. Bhunia and J. Irudayaraj, *Int. J. Food Microbiol.*, 2015, **206**, 60–66.
- 43 J. Han, L. Zhang, L. Hu, K. Xing, X. Lu, Y. Huang, J. Zhang, W. Lai and T. Chen, *J. Dairy Sci.*, 2018, **101**, 5770–5779.
- 44 M. Chen, Z. Yu, D. Liu, T. Peng, K. Liu, S. Wang, Y. Xiong, H. Wei, H. Xu and W. Lai, *Anal. Chim. Acta*, 2015, **876**, 71–76.

